Design of MPC-based Controller for a Generalized Energy Storage System Model

Álvaro Ortega, *Student Member, IEEE*, Paul Mc Namara, *Member, IEEE*, Federico Milano, *Senior Member, IEEE*

***Abstract*— This paper presents a control strategy based on Model Predictive Control for Energy Storage Systems. The mathematical formulation of this controller is outlined, and the procedure for applying this controller to a Generalized Energy Storage model is then documented. The dynamic performance of the control strategy presented is compared with that of a PI-based control technique. A comprehensive case study based on the New England 39-bus 10-machine test system with the inclusion of Energy Storage Systems is presented and discussed.**

I. Introduction

The control strategy that has been most widely applied to Energy Storage Systems (ESSs) is the PI, due mainly to its simplicity and ease of implementation. However, the performance of PI controllers can be affected by changes in system operating points and/or topology. Hence, alternative control strategies have been proposed in the literature, such as Model Predictive Control (MPC) and H-infinity Control (H_∞), among others [reference/s?]. This paper discusses the mathematical formulation and application of a MPC-based controller for a Generalized Energy Storage System (GESS) model. The dynamic behavior of this controller is compared with that of a PI-based regulator, in terms of their disturbance rejection performance over short- and medium-term time scales.

Research interest in ESSs has grown steadily in the last decade. Improved PI-based ESS controllers, capable of simultaneously regulating both the active and reactive power for Superconducting Magnetic Energy Storage (SMES) and Flywheel Energy Storage (FES) applications, are presented in [1] and [2], respectively. In [3], current control for a novel axial flux permanent magnet machine based on MPC is presented, and its performance is compared with that of a PI current controller. Finally, in [4] a constrained MPC-based frequency control scheme is derived for a simplified basic model of ESSs that considers only the state of charge of the storage device

Despite the vast literature on the topic, there is still no agreement on a general purpose – yet detailed – model for ESSs. The variety of available models is one of the reasons for a lack of systematic comparison of the different available control strategies. In this paper, all controllers are designed using the GESS model proposed in [5]. This model is briefly outlined in Section II. This is a fundamental frequency model that includes the relevant DC side dynamics of the Voltage Sourced Converter (VSC). The proposed model is tailored for the time scales considered in this work [6]–[8]. More detailed models of the VSC and controllers associated with the ESS, could be considered, e.g., the electro-magnetical models proposed in [9]. However, such models are too computationally demanding for transient stability analysis of large interconnected power systems.

The contributions of this paper are twofold, providing the following:

- A detailed description of the design and formulation of PI and MPC-based control strategies for the GESS model. This model represents the behaviour of most VSC-based ESSs with a high degree of accuracy.
- A fair and comprehensive comparison of the dynamic response of the aforementioned control strategies. The aim of the case study is to define the performance of the controllers against various contingencies and large disturbances for short- and medium-term dynamics.

II. Modelling of the Energy Storage System

Figure 1 illustrates the coupling of an ESS to an AC grid. The ESS aims to regulate a measured system signal, w, (e.g., the frequency of the center of inertia, or the active power flowing through a transmission line). The VSC is modeled using the balanced, fundamental frequency model proposed in [6]–[8], which includes DC circuit and phase-locked loop dynamics as well as an average quasi-static phasor model of the converter and an equivalent model for switching losses.

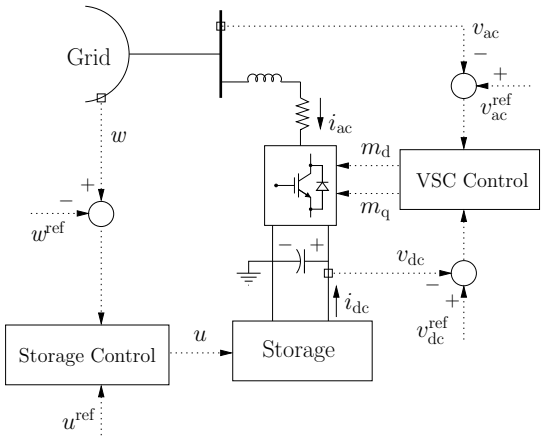

Fig. 1: Scheme of the ESS connected to a grid.

Model of the Generalized Energy Storage System

A GESS model is considered in this paper. Such a model is based on the observation that most ESSs include potential

TABLE I: Examples of energy storage technologies.

Types of Storable Energy	Potential Var.	Flow Var.	Device
Magnetic	Magneto Motive Force	Flux	SMES
Fluid	Pressure	Mass Flow	CAES
Electrostatic	Electric Potential	Electric Current	ECES
Electrochemical	Electrochemical Potential	Molar Flow Rate	BES
Rotational	Angular Velocity	Torque	FES

and flow variables (see Table I), and are connected to the grid through a VSC device. The storage devices are thus modeled as a dipole connected to the dc side of the VSC, as in Fig. 1. The main advantages of this model are its linear structure and fixed number of Differential Algebraic Equations (DAEs) for all storage technologies. With regards to both features, a range of simplifications are employed in the formulation and implementation of the control strategies discussed in this paper. Despite these simplifications, the model considered in this paper appears to be accurate and approximates detailed models with greater precision than other overly simplified ESS models that can be found in the literature. A comprehensive discussion on the accuracy of this GESS is discussed in [5].

The linear time-invariant expression of the GESS is given by:

$$\begin{aligned} \boldsymbol{\Gamma}_x \dot{\boldsymbol{x}} &= \mathbf{A}_{xx}\boldsymbol{x} + \mathbf{A}_{xz}\boldsymbol{z} + \mathbf{B}_{xu}u + \mathbf{B}_{xv}v_{\mathrm{dc}} + \mathbf{K}_x \\ \boldsymbol{\Gamma}_z \dot{\boldsymbol{z}} &= \mathbf{A}_{zx}\boldsymbol{x} + \mathbf{A}_{zz}\boldsymbol{z} + \mathbf{B}_{zu}u + \mathbf{B}_{zv}v_{\mathrm{dc}} + \mathbf{K}_z \\ i_{\mathrm{dc}} &= \mathbf{C}_x\boldsymbol{x} + \mathbf{C}_z\boldsymbol{z} + \mathbf{D}_u u + \mathbf{D}_v v_{\mathrm{dc}} + \mathbf{K}_i \end{aligned} \tag{1}$$

where the state vector $\boldsymbol{x}$ are the potential and flow variables related to the energy stored in the ESS shown in Table I, while $\boldsymbol{z}$ stands for all other variables; u is the output signal of the storage control; v_{dc} and i_{dc} are the dc voltage and current of the VSC, respectively; and $\boldsymbol{\Gamma} = \mathrm{diag}[\boldsymbol{\Gamma}_x \ \boldsymbol{\Gamma}_z]$ is a diagonal matrix such that [10]:

$\Gamma_{ii} = 1$ if the i-th equation of $[\boldsymbol{x}^T \ \boldsymbol{z}^T]^T$ is differential;
$\Gamma_{ii} = 0$ if the i-th equation of $[\boldsymbol{x}^T \ \boldsymbol{z}^T]^T$ is algebraic.

Note that u, v_{dc} and i_{dc} are scalar, whereas all other quantities are vectors.

The dynamic order of (1) is reduced, assuming that the transient response of the variables in $\boldsymbol{z}$ are much faster than those of $\boldsymbol{x}$ (i.e., $\boldsymbol{\Gamma}_z = \mathbf{0}$). Therefore, after computing the Schur components of $\boldsymbol{z}$, and rewriting the matrices in compact form, the following set of three DAEs is obtained:

$$\begin{aligned} \tilde{\boldsymbol{\Gamma}}\dot{\boldsymbol{x}} &= \tilde{\mathbf{A}}\boldsymbol{x} + \tilde{\mathbf{B}}_u u + \tilde{\mathbf{B}}_v v_{\mathrm{dc}} + \tilde{\mathbf{K}}_x \\ i_{\mathrm{dc}} &= \tilde{\mathbf{C}}\boldsymbol{x} + \tilde{\mathbf{D}}_u u + \tilde{\mathbf{D}}_v v_{\mathrm{dc}} + \tilde{\mathbf{K}}_i \end{aligned} \tag{2}$$

Finally, the energy stored in the device can be computed as follows:

$$E = \sum_{\mathrm{i}=1}^{n} \rho_{\mathrm{i}} \left(x_{\mathrm{i}}^{\beta_{\mathrm{i}}} - \chi_{\mathrm{i}}^{\beta_{\mathrm{i}}} \right) \tag{3}$$

where ρ_{i}, β_{i} and χ_{i} are the proportional coefficient, exponential coefficient and reference potential value of each variable x_{i}, respectively.

The steps involved in setting up each of the control strategies considered in this paper are as follows:

- The main parameters of the ESS are defined through detailed modeling of the device using data provided from manufacturers.
- The matrices of the GESS are obtained using the process explained above.
- The control strategies are based on the GESS model, and tested through time domain simulations.
- Finally, the controller can be directly implemented for the original detailed model of the storage device.

III. Control Strategies for ESSs

This section provides a detailed description of the mathematical formulation and practical implementation of the two control strategies considered in this work, namely PI (subsection III-A) and MPC (subsection III-B).

A. PI Control

A common scheme of a PI-based controller for ESSs is depicted in Fig. 2. This controller takes the deviations of a measured variable of the system, w, and is typically composed of a dead-band block, a low pass filter, a PI regulator, and a block referred to as the Energy Limiter, designed to disconnect the storage device if one of the energy limits is reached.

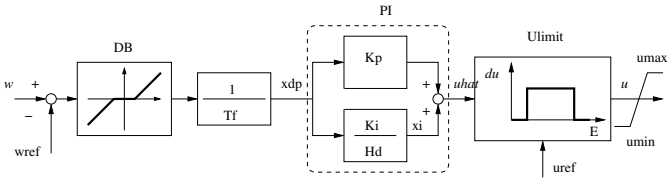

Fig. 2: PI-based storage control scheme.

In Fig. 2, the PI controller is composed of a proportional gain, $K_{\mathrm{p}u}$, and an integrator with gain $K_{\mathrm{i}u}$ and integral deviation coefficient d_{i}. Typically these gains are calculated using trial-and-error or pole-placement techniques. Therefore, the main advantages of this controller are the ease with which it is implemented in power system simulation software, and the simplicity of the design process involved. However, some research has shown how changes in system topology, as well as a shift in operation point from the one for which the PI was designed, may affect the performance of the overall system. In some cases, these changes may lead to instability [11]. This fact has inspired the development of more advanced and robust control techniques aimed to substitute or improve PI regulators [ref/s?]. One example of these alternative controllers is MPC, which is described in the remainder of this section.

B. Model Predictive Control

MPC is an optimisation-based control technique that uses state-space based predictions to form optimal inputs to a system over a prediction horizon [12]. While inputs are calculated over the full prediction horizon, only the input for the first sample step of the prediction horizon is applied to the system, and this process is repeated every sample step.

Consider a system consisting of n non-overlapping subsystems. A discrete-time, linear, time-invariant state-space model for this system is given by

$$\begin{aligned} \boldsymbol{x}_{\mathrm{d}}(k+1) &= \mathbf{A}_{\mathrm{d}}\boldsymbol{x}_{\mathrm{d}}(k) + \mathbf{B}_{\mathrm{d}}\boldsymbol{u}_{\mathrm{d}}(k) \\ \boldsymbol{y}_{\mathrm{d}}(k) &= \mathbf{C}_{\mathrm{d}}\boldsymbol{x}_{\mathrm{d}}(k) \end{aligned} \tag{4}$$

where: $\boldsymbol{x}_{\mathrm{d}}(k)$, $\boldsymbol{u}_{\mathrm{d}}(k)$, and $\boldsymbol{y}_{\mathrm{d}}(k)$ are the states, inputs, and outputs of the system at sample step k, respectively. Matrices $\mathbf{A}_{\mathrm{d}}$, $\mathbf{B}_{\mathrm{d}}$, and $\mathbf{C}_{\mathrm{d}}$ are the relevant state-space matrices. An augmented state-space model allows these equations to be framed in terms of $\Delta\boldsymbol{u}_{\mathrm{d}}(k)$ and the augmented state $\boldsymbol{\chi}_{\mathrm{d}}(k)=[\Delta\boldsymbol{x}_{\mathrm{d}}^{\mathrm{T}}(k)\ \boldsymbol{x}_{\mathrm{d}}^{\mathrm{T}}(k)]^{\mathrm{T}}$ (for a general variable $b(k)$, $\Delta b(k)=b(k)-b(k-1)$, i.e., the Δ operator denotes the change in a variable between sample steps $k-1$ and k), which ensures integral action in the controller. This is given as follows:

$$\begin{aligned} \boldsymbol{\chi}_{\mathrm{d}}(k+1) &= \hat{\mathbf{A}}_{\mathrm{d}}\boldsymbol{\chi}_{\mathrm{d}}(k) + \hat{\mathbf{B}}_{\mathrm{d}}\Delta\boldsymbol{u}_{\mathrm{d}}(k) \\ \boldsymbol{y}_{\mathrm{d}}(k+1) &= \hat{\mathbf{C}}_{\mathrm{d}}\boldsymbol{\chi}_{\mathrm{d}}(k+1) \end{aligned} \tag{5}$$

where $\hat{\mathbf{A}}_{\mathrm{d}}$, $\hat{\mathbf{B}}_{\mathrm{d}}$, and $\hat{\mathbf{C}}_{\mathrm{d}}$ are the incremental state-space matrices. The predicted state $\boldsymbol{x}_{\mathrm{p}}(k+1)$ and incremental predicted state $\Delta\boldsymbol{x}_{\mathrm{p}}(k+1)$ can be found from these equations, where for a general vector $\boldsymbol{\gamma}$, its prediction vector is $\boldsymbol{\gamma}_{\mathrm{p}}(k) = [\boldsymbol{\gamma}^{\mathrm{T}}(k)\ldots\boldsymbol{\gamma}^{\mathrm{T}}(k+H-1)]^{\mathrm{T}}$, where H is called the prediction horizon for the system [13].

MPC problems are constructed to fulfill control objectives for a system based on knowledge of $\boldsymbol{x}_{\mathrm{d}}(k)$. A cost function, $J(\boldsymbol{\chi}_{\mathrm{d}}(k), \Delta\boldsymbol{u}_{\mathrm{p}}(k))$ (which will henceforth be denoted by $J(k)$), is designed so as to embody the system's objectives. Typically this cost function is quadratic in $\Delta\boldsymbol{u}_{\mathrm{p}}$ and in this paper the cost function takes the following form:

$$J(k) = \boldsymbol{e}_{\mathrm{p}}^{\mathrm{T}}\mathbf{Q}_{\mathrm{e}}\boldsymbol{e}_{\mathrm{p}} + \boldsymbol{u}_{\mathrm{p}}^{\mathrm{T}}\mathbf{Q}_{\mathrm{u}}\boldsymbol{u}_{\mathrm{p}} + \Delta\boldsymbol{u}_{\mathrm{p}}^{\mathrm{T}}\mathbf{Q}_{\mathrm{du}}\Delta\boldsymbol{u}_{\mathrm{p}} \tag{6}$$

where the $(k+1)$ dependency is dropped from $\boldsymbol{e}_{\mathrm{p}}(k+1)$, and the (k) dependency is dropped from $\Delta\boldsymbol{u}_{\mathrm{p}}(k)$ and $\boldsymbol{u}_{\mathrm{p}}(k+1)$ in (6) for compactness. The error vector, $\boldsymbol{e}_{\mathrm{p}}(k)=\boldsymbol{y}_{\mathrm{p}}(k)-\boldsymbol{r}_{\mathrm{p}}(k)$, where $\boldsymbol{r}(k)$ are the setpoints of the system at sample step k. The weighting matrices $\mathbf{Q}_{\mathrm{e}}$, $\mathbf{Q}_{\mathrm{u}}$, and $\mathbf{Q}_{\mathrm{du}}$ determine the relative importance of minimizing the error, the change in the input from it's original nominal value, and the incremental changes in inputs, respectively. Once (6) is solved for $\Delta\boldsymbol{u}_{\mathrm{p}}(k)$, $\boldsymbol{u}(k)$ is applied to the system, and the MPC process is conducted each sample step. In this paper (6) is solved in an unconstrained fashion and thus the control law is effectively a fixed gain feedback law and can be computed in a highly efficient fashion. Unconstrained MPC in this form is equivalent in performance to a finite horizon Linear Quadratic Regulator.

Note that in the above formulation MPC is carried out from a central location. At each sample step the controller must have access to the full state-space of the system to formulate the control problem.

Finally, MPC is applied to the ESS model in Subsection II by applying the following designations:

- $\boldsymbol{x}_{\mathrm{d}}(k)$ are the states of the full system, i.e., the grid, the VSC device and its controllers, and the storage device;
- $\boldsymbol{u}_{\mathrm{d}}(k)$ is the input variable of the storage device, u (see Fig. 1);
- $\boldsymbol{y}_{\mathrm{d}}(k)$ is the measured signal of the grid to be regulated, w.

IV. Case Study

In this section, a performance comparison is made between the two control strategies for ESSs discussed in this paper, namely the PI and MPC schemes. The study is based on the well-known New England 39-bus 10-machine test system. This benchmark network contains 19 loads totaling 6097.1 MW and 1409.1 MVAr of active and reactive power, respectively. The system model also includes generator controllers such as primary voltage regulators, as well as both primary and secondary frequency regulation (turbine governors and an AGC). Three identical storage devices are considered in this paper, and are connected to buses 2, 11 and 19. The maximum power output of each ESS is 30 MW, the time step of the MPC regulator is 0.5 s, and the prediction horizon is 60 samples. All dynamic data of the New England 39-bus 10-machine system can be found in [14].

Two main scenarios have been considered in this paper: Subsection IV-A shows the response of the system facing a line outage cascade for the base case load condition, whereas in Subsection IV-B a similar analysis is carried out for a 20% of overload in the system.

All simulations and plots have been obtained using Dome [15]. Dome has been compiled based on Python 3.4.2, CVXOPT 1.1.8, SuiteSparse 4.4.5, ATLAS 3.10.2, and Matplotlib 1.4.3; and has been executed on a 64-bit Linux Ubuntu 12.04 distribution running on 8 core 3.60 GHz Intel Xeon with 12 GB of RAM.

A. Base Case Load Condition

In this subsection, a line outage cascade is simulated. Specifically, the line that connects buses 16 and 21 is disconnected at $t = 1$ s, followed by the outage of the line connecting buses 26 and 27 at $t = 30$ s. The system variable regulated by the ESSs is the frequency of the Centre of Inertia (COI), and its response is depicted in Fig. 3(a). It can be seen that both the PI and the MPC controllers are able to reduce the frequency variations by about 90%. For a fair comparison, both controllers have been tuned in order to obtain a similar performance. The power consumed/provided by the ESS connected to bus 2 is represented in Fig. 3(b). The other ESSs show a similar behaviour. Note that the ESS uses load notation. Thus, the ESS stores energy for positive values of the power, and vice versa. It can be observed how the discontinuities of the MPC control cause fast power oscillations during the transients.

B. 20% Overload

This subsection discusses the performance of the two control strategies when the operating conditions differ from those for which the controllers were designed. With this aim, a 20% overload is simulated (see Fig. 4). Control parameters are the

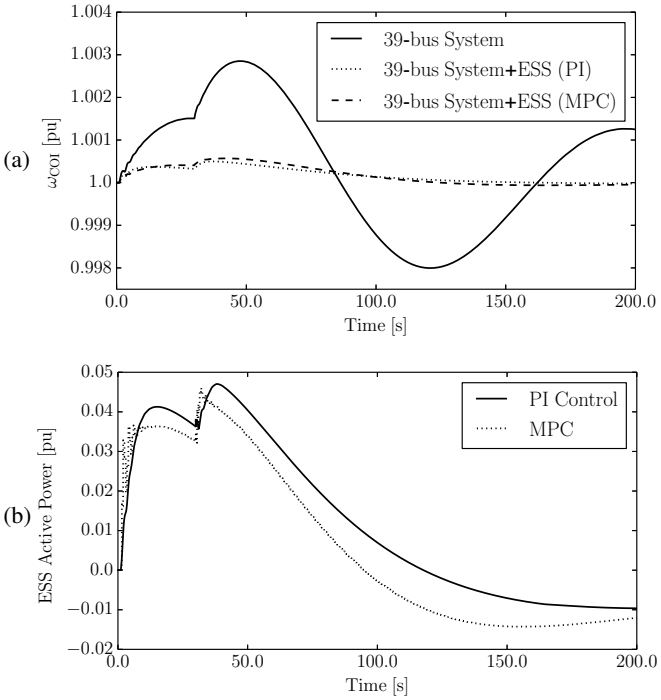

Fig. 3: Response of the 39-bus system with three ESSs following a line outage cascade. (a) Frequency of the COI (b) Active power of the ESS at bus 2.

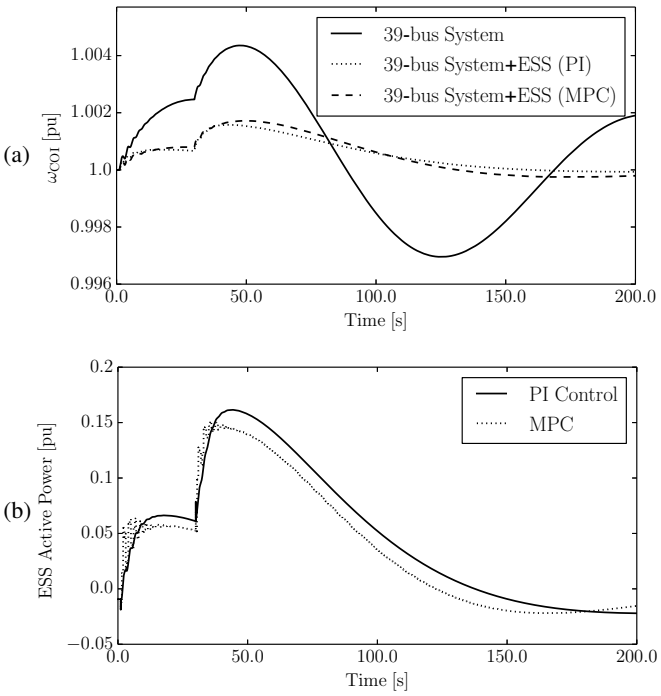

Fig. 4: Response of the 39-bus system with three ESSs following a line outage cascade with a 20% of overload. (a) Frequency of the COI (b) Active power of the ESS at bus 2.

same as those used in the base case example. Figure 4(a) shows that the behaviour of both controllers is similar. The PI appears to reach the steady-state slightly faster. However, Fig. 4(b) shows how the PI requires a larger amount amount

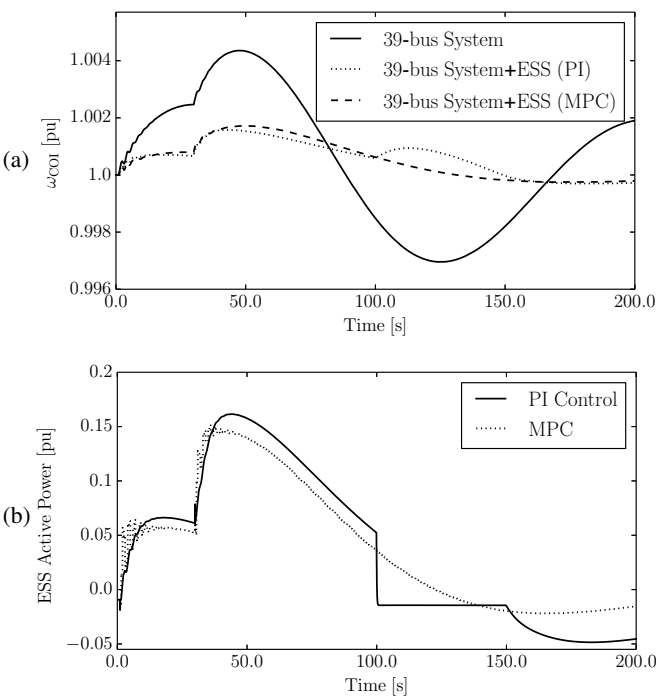

Fig. 5: Response of the 39-bus system with three ESSs close to their upper energy limits and following a line outage cascade with a 20% of overload. (a) Frequency of the COI (b) Active power of the ESS at bus 2.

of active power than the MPC for regulation. This fact can be relevant if storage energy limits are considered, as shown in Fig. 5.

In Fig. 5, the initial states of charge (SoC) of the ESSs are set close to their maximum value. The same values for the initial SoC and upper limits are chosen for both the PI and the MPC controllers. Figures 5(a) and 5(b) show that the energy saturation leads to an abrupt step in the active power of the ESS with PI control at about $t = 100$ s. Once the energy limit is reached, a frequency oscillation appears. The amplitude of such an oscillation is similar to that caused by the line outage. On the other hand, the MPC is able to predict the future state of the system, providing a better usage of the active power of the storage device and thus avoiding energy saturations. Thus, the MPC prevents the frequency oscillations shown by the PI controller.

Finally, a three-phase fault at bus 21 at $t = 1$ s is simulated to observe the performance of the two controllers subject to large disturbances. The fault is cleared after 80 ms by opening line connecting buses 16 and 21, followed by the cascade phenomena with the line connecting buses 26 and 27 at $t = 30$s. Energy saturations of the storage devices are not considered in this case. The frequency of the COI and the active power of the ESS connected to bus 2 are shown in Figs. 6(a) and 6(b), respectively. It can be seen that both controllers are able to reduce the frequency deviations during and after the transients. However, large active power oscillations are present in the case of the MPC. Such oscillations last about 20 s and are due to the discontinuous behavior of the MPC.

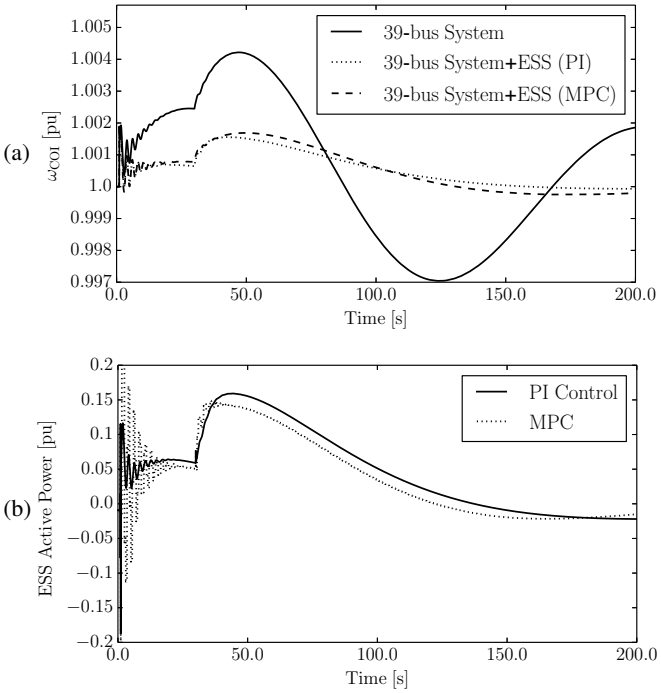

Fig. 6: Response of the 39-bus system with three ESSs following a fault and line outage cascade with a 20% of overload. (a) Frequency of the COI (b) Active power of the ESS at bus 2.

Decreasing the sampling time of the MPC discretization can reduce oscillations, but increases the computational burden of the MPC. Another way to prevent the occurrence of oscillations is to increase the weight associated with the control effort. However, this way will result in a poorer performance for medium to long term transients.

V. Conclusions

This paper presents an advanced control strategy based on MPC for a GESS model. The mathematical formulation and design of the storage device model and MPC-based controller, are duly discussed. The dynamic performance of the proposed controller is compared with a PI-based regulator. Simulation results show that there advantages and disadvantages associated with both approaches. The MPC-based regulator proves to have more desirable medium and long term behavior, whereas the PI-based controller provides better regulation during the transients. The PI controller is more sensitive to energy saturations than the MPC, too.

Since the centralized approach for MPC may be impractical for large-scale systems, or for systems composed of a number of different areas, decentralized or distributed approaches must be considered. This will be addressed in future work. Other relevant topics that will be considered for future work are the inclusion of constraints to limit the power output of storage devices, as well as the development of strategies to coordinate ESSs according to their sizes and current states of charge.

Acknowledgments

This material is based upon works supported by the Science Foundation Ireland, by funding F. Milano, under Grant No. SFI/09/SRC/E1780. The opinions, findings and conclusions or recommendations expressed in this material are those of the authors and do not necessarily reflect the views of the Science Foundation Ireland. P. Mc Namara and F. Milano are also funded under the Programme for Research in Third Level Institutions and co-funded under the European Regional Development Fund (ERDF). F. Milano is also a beneficiary of financial support from the EC Marie Skłodowska-Curie Career Integration Grant No. PCIG14-GA-2013-630811.

References

[1] M. G. Molina, P. E. Mercado, and E. H. Watanabe, "Improved Superconducting Magnetic Energy Storage (SMES) Controller for High-Power Utility Applications," *IEEE Transactions on Energy Conversion*, vol. 26, no. 2, pp. 444 – 456, June 2011.

[2] G. Li, S. Cheng, J. Wen, Y. Pan, and J. Ma, "Power System Stability Enhancement by a Double-fed Induction Machine with a Flywheel Energy Storage System," in *Power Engineering Society General Meeting, IEEE*, Montreal, Que, 2006.

[3] T. D. Nguyen, K. J. Tseng, S. Zhang, S. Zhang, and H. T. Nguyen, "Model predictive control of a novel axial flux permanent magnet machine for flywheel energy storage system," in *IPEC, 2010 Conference Proceedings*, Oct 2010, pp. 519–524.

[4] C. Trabert, A. Ulbig, and G. Andersson, "Model predictive frequency control employing stability constraints," in *American Control Conference (ACC), 2015*, July 2015, pp. 5678–5685.

[5] Á. Ortega and F. Milano, "Generalized Model of VSC-based Energy Storage Systems for Transient Stability Analysis," *IEEE Transactions on Power Systems*, 2015, (in press). [Online]. Available: arXiv:1509.05290

[6] D. N. Kosterev, "Modeling Synchronous Voltage Source Converters in Transmission System Planning Studies," *IEEE Transactions on Power Delivery*, vol. 12, no. 2, pp. 947–952, Apr. 1997.

[7] E. Uzunovic, C. A. Cañizares and J. Reeve, "Fundamental Frequency Model of Static Synchronous Compensator," in *29th North American Power Symposium (NAPS)*, Laramie, Wyoming, Oct. 1997, pp. 49–54.

[8] E. Acha and B. Kazemtabrizi, "A New STATCOM Model for Power Flows Using the NewtonRaphson Method," *IEEE Transactions on Power Systems*, vol. 28, no. 3, pp. 2455–2465, Aug. 2013.

[9] A. Yazdani and R. Iravani, *Voltage-Sourced Converters in Power Systems. Modeling, Control and Applications*, 1st ed. Wiley-IEEE Press, 2010.

[10] P. Aristidou, D. Fabozzi, and T. V. Cutsem, "Dynamic Simulation of Large-Scale Power Systems Using a Parallel Schur-Complement-Based Decomposition Method," *IEEE Transactions on Parallel and Distributed Systems*, vol. 25, no. 10, pp. 2561–2570, Oct. 2014.

[11] A. Etxeberria, I. Vechiu, H. Camblong, and J.-M. Vinassa, "Comparison of Sliding Mode and PI Control of a Hybrid Energy Storage System in a Microgrid Application," in *International Conference on Smart Grid and Clean Energy Technologies*, Chengdu, China, Sept. 2011, pp. 966–974.

[12] P. Mc Namara, R. Meere, T. O'Donnell, and S. McLoone, "Distributed MPC for Frequency Regulation in Multi-Terminal HVDC Grids," in *IFAC World Congress*, vol. 19, no. 1, Cape Town, South Africa, 24-29 Aug. 2014, pp. 11 141–11 146.

[13] J. Maciejowski, *Predictive Control with Constraints*. Harlow, England: Prentice Hall, 2002.

[14] Illinois Center for a Smarter Electric Grid (ICSEG), "IEEE 39-Bus System," URL: http://publish.illinois.edu/smartergrid/ieee-39-bus-system/.

[15] F. Milano, "A Python-based Software Tool for Power System Analysis," in *Procs. of the IEEE PES General Meeting*, Vancouver, BC, July 2013.